Engineering and Technology Journal e-ISSN: 2456-3358
Volume 09 Issue 10 October-2024, Page No.- 5293-5304
DOI: 10.47191/etj/v9i10.05, I.F. – 8.227

Comparative Corrosion Inhibition Test Study in Phosphate Buffer Saline for 316L Stainless Steel with Electrospun PCL Coating with Different Additives

Ersin Kamberli[1,*], Mothana Ghazi Kadhim AlFalah[2], Fatma Kandemirli[3]
[1,3]Biomedical Engineering, Kastamonu University, Faculty of Enginnering and Architecture, Kastamonu, Türkiye
[2]Materials of Engieering Department, College of Engineering, University of Al–Qadisiyah, 58002, Al–Qadisiyah, Iraq
(https://orcid.org/0000-0001-9047-4274)[1], (https://orcid.org/0000-0002-8970-712X)[2], (https://orcid.org/0000-0001-6097-2184)[3]

ABSTRACT: In this study, ten different contents of PCL-based nanofibers containing ZnO, CuO, NiO, 2F TSC, 4F TSC and graphite additives (PCL+Graphite+CuO+NiO+ZnO, PCL+ZnO+Graphite, PCL+ZnO+NiO+CuO, PCL+ZnO, PCL+Graphite, PCL+ZnO+2F TSC, PCL+ZnO+NiO+CuO+4F TSC, PCL+ZnO+NiO+CuO+2F TSC, bare PCL, PCL+ZnO+4F TSC) 316L stainless steel (SS) surface was coated. After coating with these different types of nanofibers, measurements were taken with electrochemical techniques such as potentiodynamic polarization (PDP) and electrochemical impedance spectroscopy (EIS) in phosphate buffer solution (PBS) for 1 hour to investigate the corrosion inhibition properties. According to the results, the PCL+Graphite+CuO+NiO+ZnO coating provided the highest corrosion inhibition with a protection efficiency value of 98.83%. The PCL+4F+ZnO coating had the lowest inhibition property with a protection efficiency value of 40.72%. At the end of the tests, Nyquist, Bode, Tafel, OCP diagrams of the coatings were obtained and equivalent circuit models were presented.

KEYWORDS: EIS, corrosion inhibition, polymer coating

INTRODUCTION

Austenitic stainless steel (316L SS) has recently gained recognition as a promising material for bone implants due to its exceptional corrosion resistance and beneficial mechanical properties [1, 2]. This material's outstanding performance in aqueous environments is largely due to a protective, passive layer of chromium oxide that forms naturally on its surface. This layer, enriched with chromium, serves as a barrier between the metal and potentially corrosive elements like oxygen and water. While the passive layer's thickness and makeup can differ based on environmental factors, it generally remains robust and adherent, offering durable protection. Nevertheless, 316L SS is not without its drawbacks, such as its susceptibility to pitting corrosion, which can lead to the release of metal ions like nickel, chromium, and molybdenum, potentially impacting the material's biocompatibility and longevity [3]. To mitigate these issues, researchers have explored surface modification techniques, including composite coatings that combine various materials to enhance the implant's protective qualities. Polymer coatings, in particular, have shown promise in safeguarding 316L SS implants from corrosion in simulated bodily fluids [4-6]. Additionally, nanofibers are gaining traction across various fields, including medical devices and filtration, with numerous production methods available, such as electrospinning, which employs electrostatic forces to create fibers from micro- to nanoscale. The technique employs a strong electric field applied between two electrodes carrying opposite charges to regulate fiber formation. Electrospinning has garnered substantial interest for its precise control over fiber characteristics such as shape, dimensions, and structure. This method is also highly adaptable and scalable, capable of processing a diverse array of materials, which makes it a compelling choice for scientists and engineers across multiple disciplines [7].

Polycaprolactone (PCL) and gelatin are utilized as coatings for bone implants and cardiovascular stents, enhancing the functionality of these devices by improving cell viability and biocompatibility. Organic coatings like polycaprolactone are favored for modifying implant surfaces because they create a stable and compatible interface with surrounding tissues. PCL, an aliphatic polyester with semi-crystalline properties, belongs to a class of resorbable polymers that are promising for medical use due to their compatibility with biological systems and their distinctive thermoplastic characteristics. A key benefit of PCL is its gradual degradation through water absorption and hydrolysis, which releases biocompatible by-products that can be incorporated into metabolic processes or safely excreted. Despite these benefits, PCL also has limitations as an implant coating material; its synthetic nature results in low surface

wettability and a lack of functional surface groups crucial for effective biomedical applications, especially for coatings [8].

Steel alloys are widely utilized in construction for their superior mechanical properties and strength, coupled with their affordability and rapid production capabilities. Nonetheless, to prevent expensive damage and resource loss, it is crucial to protect these materials from corrosion [9]. In industrial and commercial environments, corrosion can lead to substantial damage, costly repairs, and operational interruptions. To address these issues, applying corrosion-resistant coatings has emerged as a highly cost-effective and efficient method for controlling corrosion. These coatings create a protective barrier between the metal and its environment, shielding the surface from corrosive agents like oxygen and chemicals. They can be customized to suit specific environmental challenges, such as high humidity or chemical exposure, and offer a robust defense against corrosion. Implementing these coatings helps prolong the lifespan of steel structures and minimizes maintenance expenses over time [10-12]. Advances in surface engineering have recently led to the development of various surface treatments and coatings that significantly improve the corrosion resistance of metallic materials [13].

Recent developments in nanotechnology have enabled the creation of nanofibers with precise control over their shape and structure, enhancing their suitability for various practical uses. A notable technique in this domain is electrospinning, which has become increasingly popular in recent years [13]. This process allows for the deposition of extremely fine polymeric fibers, down to the nanoscale, onto metal surfaces [14]. Electrospun fibers have proven to be highly effective as protective barriers, significantly reducing metal corrosion rates. Additionally, the porous nature of these coatings helps to remove corrosive substances and prevent gas bubble formation, thereby improving stability [15-16]. Electrospinning is not only straightforward to implement but also versatile, economical, efficient, and scalable. It can accommodate a broad spectrum of both natural and synthetic materials, making it an excellent choice for enhancing the corrosion resistance of metal substrates [17-18]. In our previous studies, we examined the performance of nanofiber coatings made from PCL/Zn, PCL/Ni, PCL/Cu, and PCL/Zn-Ni-Cu on mild steel in acidic solutions. The most promising results were observed with PCL/Zn and PCL/Zn-Ni-Cu nanofibers; thus, further investigation of these coatings on 316L SS in PBS is recommended [19].

This study aims to assess the performance of electrospun composite nanofiber coatings on 316L stainless steel and explore their ability to inhibit corrosion in a phosphate-buffered saline (PBS) solution. To accomplish this, three distinct coatings were prepared via electrospinning: PCL (polycaprolactone), PCL/ZnO (polycaprolactone with zinc oxide), and PCL/ZnO-NiO-CuO (polycaprolactone with zinc oxide, nickel oxide, and copper oxide). These coatings were applied to the surface of the 316L stainless steel. The effectiveness of the coatings in preventing corrosion was analyzed using electrochemical methods, specifically electrochemical impedance spectroscopy (EIS).

EXPERIMENTAL

Samples and fluid preparation

For the sample preparation, a 316L stainless steel rod with a diameter of 1 cm and a length of 3 cm was used. The chemical composition of 316L stainless steel, by weight, includes C: 0.030%; Mn: 2.0%; P: 0.045%; S: 0.03%; Si: 1.0%; Cr: 16.0%-18.0%; Ni: 10.0%-14.0%; and Mo: 2.0%-3.0%. Cylindrical specimens of 1 cm in diameter and 3 cm in length were machined from this rod. The preparation procedures for the working electrode are detailed in our previous research [19]. Materials such as PCL, Cu(CO2CH3)2•H2O, Ni(OCOCH3)2•4H2O, methanol, and dichloromethane (DCM) were sourced from Sigma-Aldrich, USA, while the PBS, which includes monobasic and dibasic phosphate, distilled water and a little salt (NaCl), was prepared by self effort in our labouratory.

Coating of SS with electrospinning method

An electrospinning solution with a 10 wt. % concentration was used to produce PCL and its derivative coatings. To prepare the PCL solution, 1 gram of PCL was dissolved in 10 milliliters of dichloromethane (DCM) and methanol mixture, which constituted the initial sample. This preparation step was consistent across all samples. Further procedural details are outlined in our previous study by AlFalah et al. [19]. Each solution was stirred continuously with a magnetic stirrer for 6 hours at room temperature to ensure uniformity. The solutions were then loaded into 10 ml syringes and connected through plastic tubing to a copper nozzle with a 1 mm diameter. A high-voltage generator was used to apply a voltage of 20 kV [20-21] to the solution, leading to the formation of dense fibers that were deposited onto stainless steel to create a fibrous web. The electrospinning was performed at room temperature and controlled humidity, with a 12 cm distance between the electrode and nozzle and a flow rate of 0.01 ml/min. Each electrospinning run lasted 5 minutes.

Electrochemical corrosion tests

In this study, electrochemical testing was carried out using the CompactStat Electrochemical Instrument from Ivium Technologies. A three-electrode setup was employed, consisting of a 316L stainless steel working electrode, an Ag/AgCl reference electrode, and a platinum wire counter electrode. The electrolyte liquid was PBS. Both alternating current (AC) and direct current (DC) electrochemical techniques were utilized, including impedance spectroscopy (EIS), linear polarization resistance (LPR), and

potentiodynamic polarization (PDP). The samples were immersed in a stagnant SBF solution at room temperature for one hour to ensure a stable surface condition before testing. EIS measurements were conducted first, followed by LPR and PDP analyses. EIS measurements were recorded across a frequency range from high to low, with an applied amplitude of 0.005V. To ensure the reliability of the results, each electrochemical test was repeated at least three times. All data were adjusted to a standard surface area of 1 cm^2 for consistency in the presented graphs.

RESULTS AND DISCUSSION

Analysis Before Coating

For corrosion tests, ten different polymer nanofibrous samples were prepared by electrospinning method and are given following with their serial numbers.

1. CuO + ZnO + NiO + Graphite + PCL
2. ZnO + Graphite + PCL
3. ZnO + CuO + NiO + PCL
4. PCL + ZnO
5. PCL + Graphite
6. 2 fluorothiosemicarbazide + ZnO + PCL
7. 4 fluorothiosemicarbazide + ZnO + NiO + CuO + PCL
8. 2 fluorothiosemicarbazide + ZnO + NiO + CuO + PCL
9. PCL
10. 4 fluorothiosemicarbazide + ZnO + PCL

For ten nanofiber samples obtained by electrospinning method, water contact angle and SEM&EDX analyses were performed before corrosion tests.

Water Contact Angle Analysis

The findings indicate that the water contact angles for the ten different nanofiber samples were measured as illustrated in Fig. 1. For these nanofibers, an angle exceeding 90 degrees denotes a hydrophobic property, whereas an angle below 90 degrees signifies hydrophilicity. Typically, a higher degree of hydrophobicity correlates with enhanced corrosion resistance. Based on the water contact angle measurements, the 4 fluorothiosemicarbazide + ZnO + NiO + CuO + PCL (number 7) nanofibers exhibit the most pronounced hydrophobic characteristics, followed by 2 fluorothiosemicarbazide + ZnO + PCL (number 6) nanofibers, with ZnO + Graphite + PCL (number 2) showing the least hydrophobic behavior.

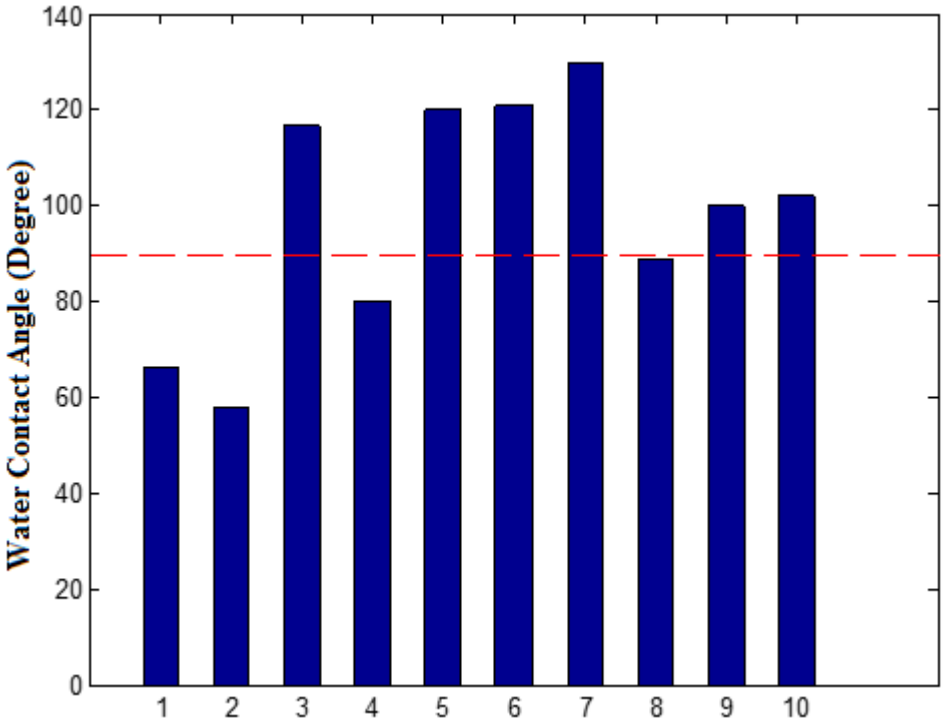

Figure – 1 Water contact angle data of samples

SEM & EDX Analysis

Scanning electron microscope images and EDX data of the samples are given in Figure 2. The magnification ratio in the images is 20,000. The C element ratio is 78.82% and the O element ratio is 21.18% by weight in the nanofibers formed with the PCL solution. In terms of atomic composition, the C element ratio is 83.21%, while the O element ratio is 16.79%. The presence of Zn is clearly seen in the EDX data of the nanofibers obtained with the PCL solution to which zinc was added. These three elements are also observed in the EDX

data of the PCL solution to which three different elements (Zn, Ni, Cu) were added. SEM and EDX data for the other samples are also given in Figure 2.

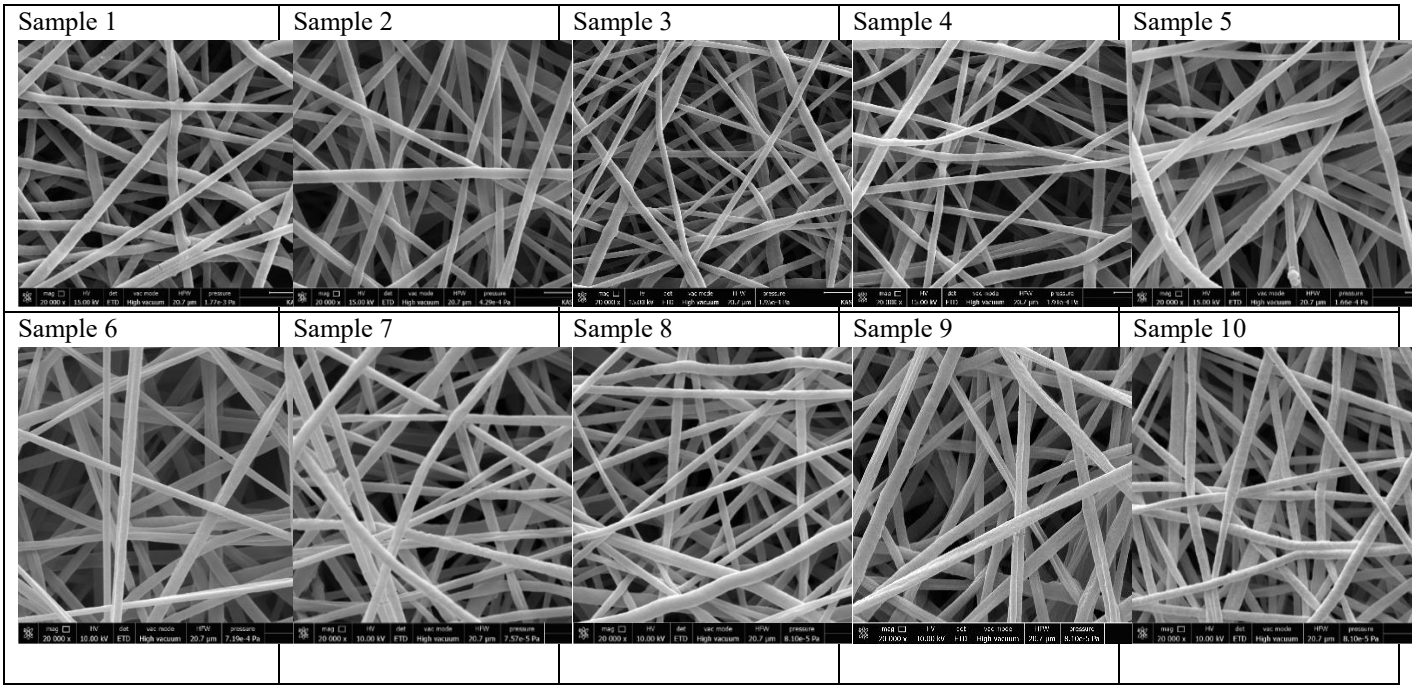

Sample 1

Element	Weight %	Atomic %	Net Int.	Error %	Kratio	Z	R	A	F
C	72.20	78.94	1219.7	4.39	0.49	1.02	0.99	0.66	1.00
O	24.92	20.46	200.6	9.88	0.03	0.97	1.01	0.14	1.00
Co	0.49	0.11	12.1	17.02	0.00	0.72	1.09	1.02	1.37
Ni	0.80	0.18	17.4	6.97	0.01	0.75	1.09	1.02	1.35
Zn	1.59	0.32	21.6	4.13	0.01	0.71	1.09	1.02	1.29

Sample 2

Element	Weight %	Atomic %	Net Int.	Error %	Kratio	Z	R	A	F
C	76.95	82.46	992.9	3.92	0.56	1.01	0.99	0.71	1.00
O	21.39	17.21	114.9	10.15	0.03	0.97	1.01	0.13	1.00
Zn	1.66	0.33	17.1	4.98	0.02	0.70	1.09	1.02	1.37

Sample 3

eZAF Smart Quant Results

Element	Weight %	Atomic %	Net Int.	Error %	Kratio	Z	R	A	F
C K	76.16	82.06	1163.5	4.01	0.54	1.01	0.99	0.70	1.00
O K	21.62	17.49	140.9	10.05	0.03	0.97	1.01	0.13	1.00
NiK	0.41	0.09	8.4	14.60	0.00	0.74	1.09	1.02	1.47
CuK	0.66	0.13	10.2	13.11	0.01	0.71	1.09	1.02	1.40
ZnK	1.15	0.23	13.8	4.69	0.01	0.70	1.09	1.02	1.33

Lsec: 522.9 0 Cnts 0.000 keV Det: Octane Pro Det

Sample 4

eZAF Smart Quant Results

Element	Weight %	Atomic %	Net Int.	Error %	Kratio	Z	R	A	F
C K	74.04	79.83	697.8	4.13	0.53	1.01	0.99	0.70	1.00
O K	24.58	19.89	102.2	10.48	0.03	0.97	1.01	0.14	1.00
ZnK	1.38	0.27	10.9	5.96	0.01	0.70	1.09	1.02	1.41

Lsec: 285.4 0 Cnts 0.000 keV Det: Octane Pro Det

Sample 5

Element	Weight %	Atomic %	Net Int.	Error %	Kratio	Z	R	A	F
C	76.51	81.27	865	3.43	0.59	1.01	1.00	0.76	1.00
O	23.49	18.73	104.9	10.11	0.03	0.96	1.01	0.13	1.00

Sample 6

Element	Weight %	Atomic %	Net Int.	Error %	Kratio	Z	R	A	F
C	80.60	85.04	1002.1	3.30	0.63	1.01	1.00	0.77	1.00
O	18.12	14.35	82.9	10.24	0.02	0.96	1.01	0.12	1.00
F	0.75	0.50	5.8	14.61	0.00	0.90	1.02	0.16	1.00
Zn	0.52	0.10	5.6	6.56	0.01	0.70	1.09	1.02	1.63

Sample 7

Sample 8

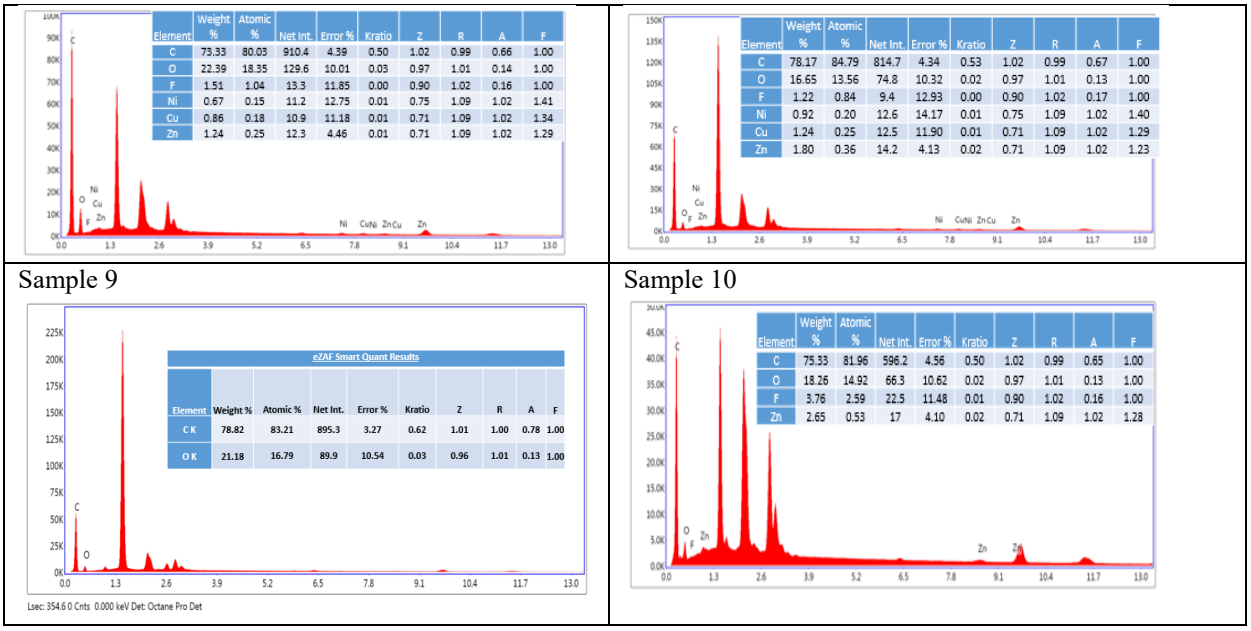

Figure 2. SEM image and EDX data of nanofiber samples

Analysis After Coating

Open Circuit Potential (OCP)

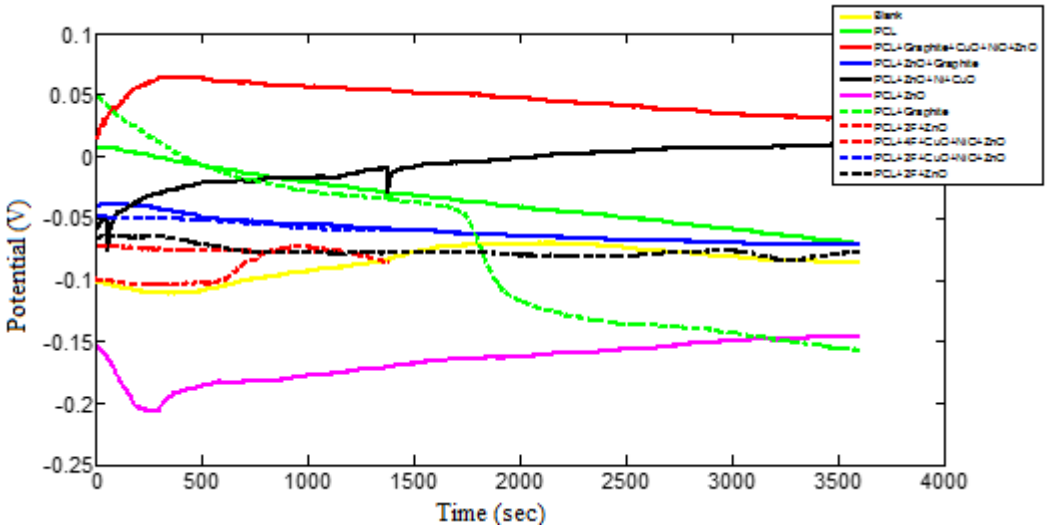

Figure 3. OCP data of nanofiber samples

Figure - 3 shows OCP data potential versus time. The PCL + ZnO sample has the lowest potential among the samples, while the PCL + graphite + ZnO + CuO + NiO sample has the highest potential. Samples' OCP graphs are not erratic or noisy, they appear like drifting type.

Nyquist & Bode & Tafel & Equivalent Circuit Analysis

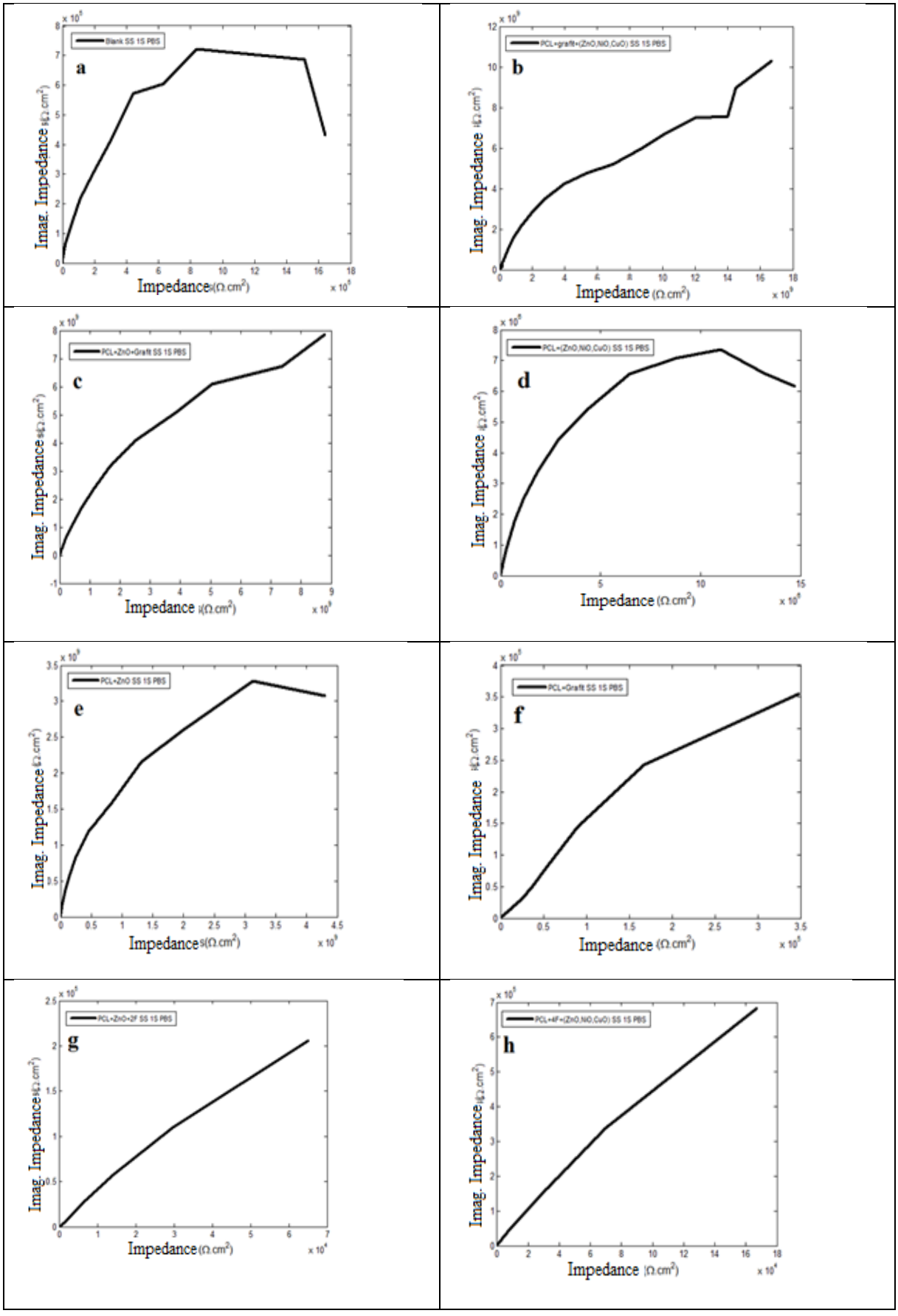

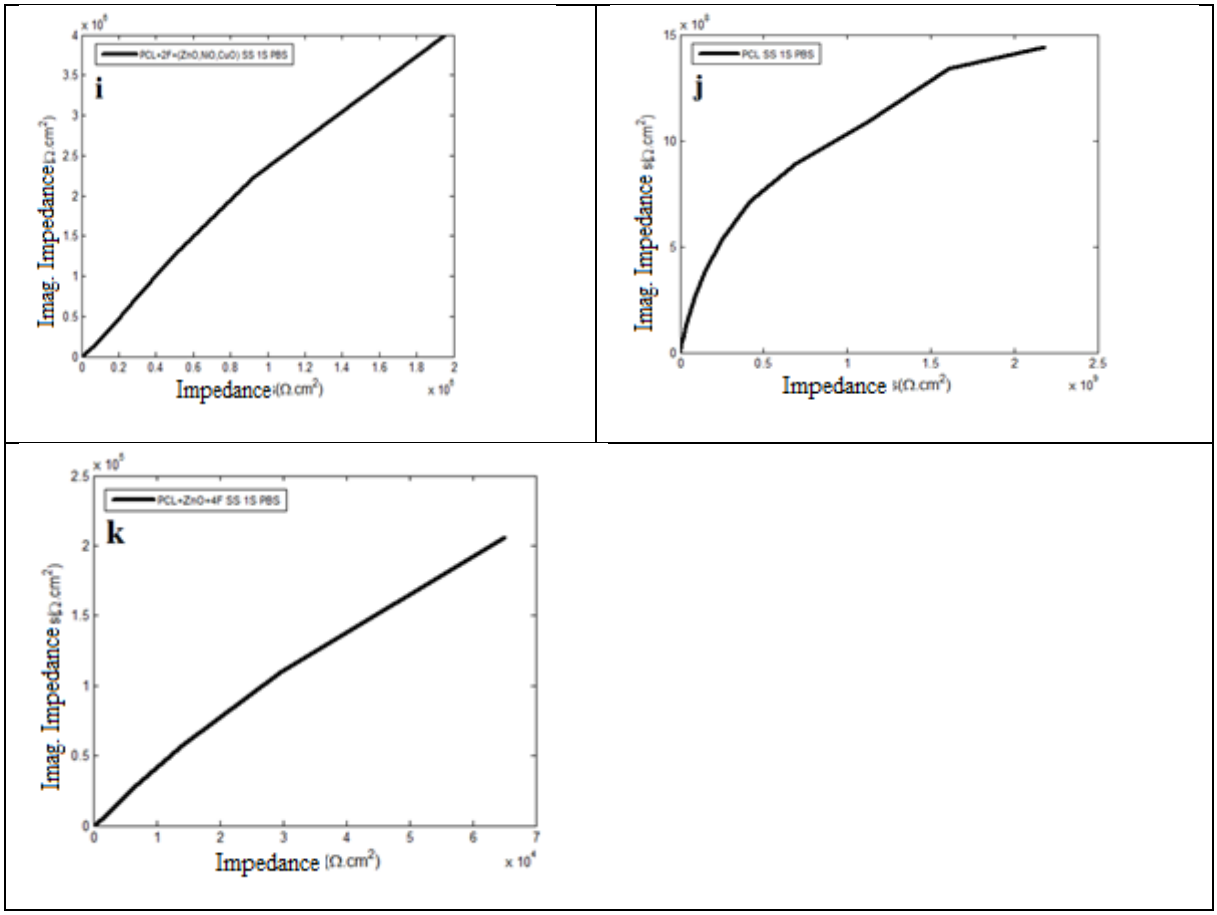

Figure 4. Impedance values of the 1-hour test of samples' on the 316L stainless steel surface in PBS; a) Blank, b) 1, c) 2, d) 3, e) 4, f) 5, g) 6, h) 7, i) 8, j) 9, k) 10

The Nyquist plot of the blank shows impedance value drastically increase in first minutes then increase rate slow down and finally decrement starts at the end of the hour. Third and fourth samples' graphs are similar to blank one. It indicates corrosion inhibition effect of coating are not very effective for third and fourth one. Other samples' impedance values are very close to each other which have trend of mostly increment during the 1 hour. Therefore, it is clear that these samples give an effective corrosion inhibition to stainless steel for 1 hour test.

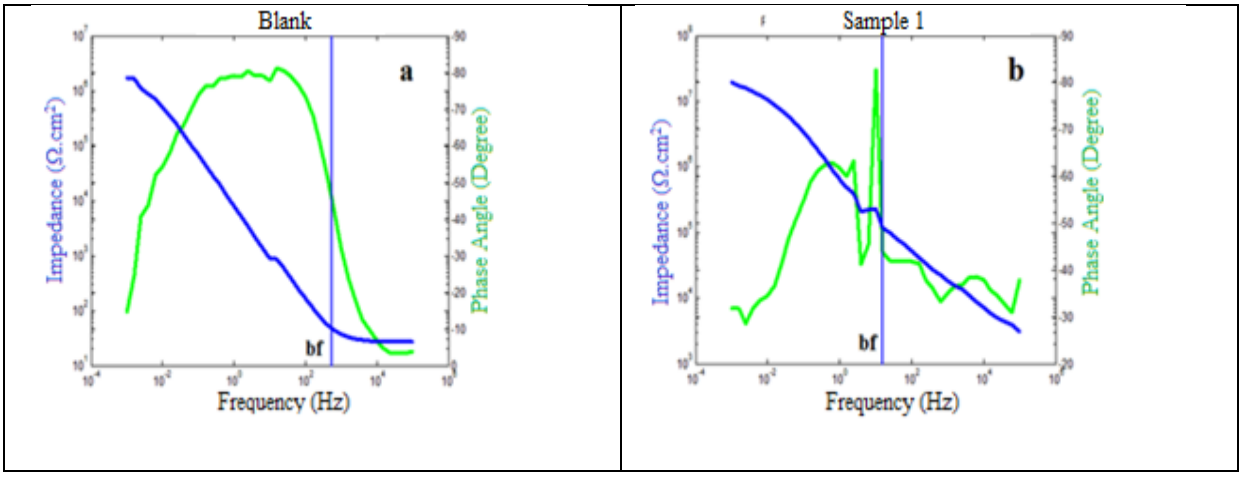

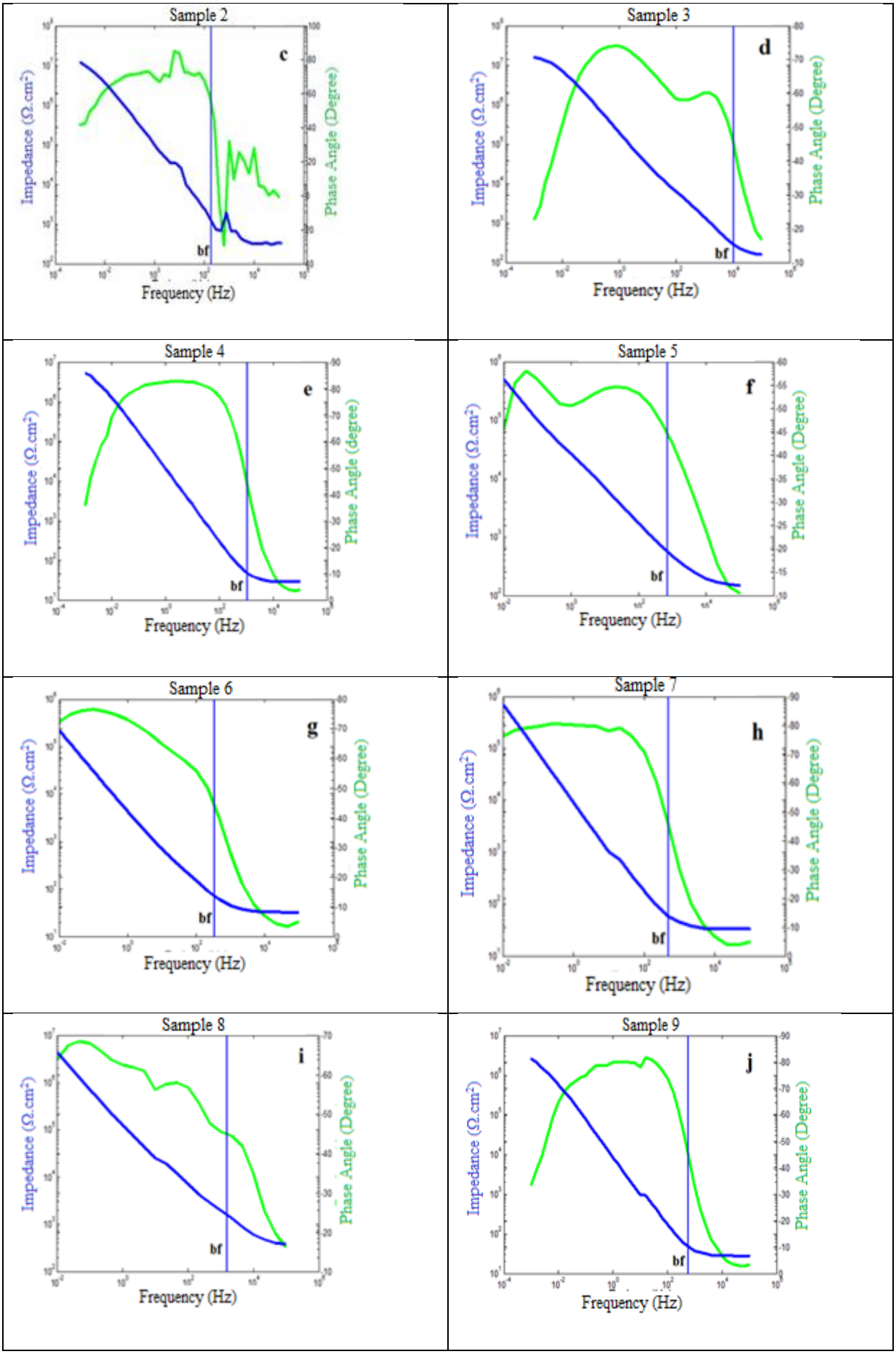
Sample 2
c
Impedance (Ω.cm²)
Phase Angle (Degree)
bf
Frequency (Hz)
Sample 3
d
Impedance (Ω.cm²)
Phase Angle (Degree)
bf
Frequency (Hz)
Sample 4
e
Impedance (Ω.cm²)
Phase Angle (degree)
bf
Frequency (Hz)
Sample 5
f
Impedance (Ω.cm²)
Phase Angle (Degree)
bf
Frequency (Hz)
Sample 6
g
Impedance (Ω.cm²)
Phase Angle (Degree)
bf
Frequency (Hz)
Sample 7
h
Impedance (Ω.cm²)
Phase Angle (Degree)
bf
Frequency (Hz)
Sample 8
i
Impedance (Ω.cm²)
Phase Angle (Degree)
bf
Frequency (Hz)
Sample 9
j
Impedance (Ω.cm²)
Phase Angle (Degree)
bf
Frequency (Hz)

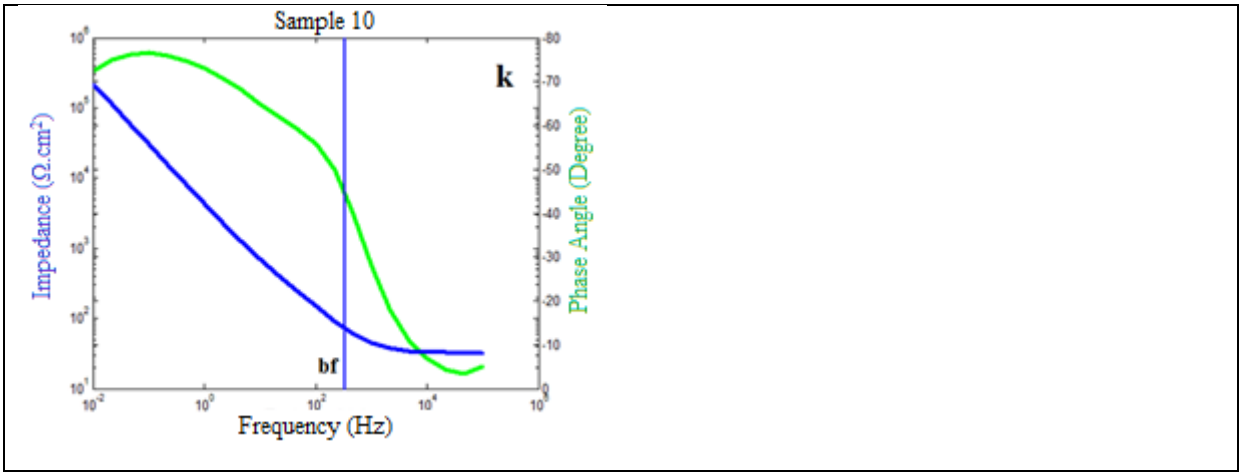

Figure 5. Impedance, phase angle frequency values and breakpoint frequency (bf) values of 1-hour measurement of samples on the 316L stainless steel surface in PBS. a) Blank, b) 1, c) 2, d) 3, e) 4, f) 5, g) 6, h) 7, i) 8, j) 9, k) 10

Examination of the Bode plot (especially breakpoint frequency) is important in demonstrating the corrosion inhibition properties of the coating. First and second samples have many fluctuations to receive the meaningful data for Bode graph. In the analysis of other graphs, the data of these graphs are more consistent and the breakpoint frequency lines more clearly divide the impedance graph into two parts

.

Table 1 Tafel data of samples

No	Sample	E_{CORR} (V)	$I_{CORR(uA/cm^2)}$	β_a	β_c	Prot. Eff%	R_{LPR} (Ω)	$Prot_{LPR}$. Eff%
	BLANK	-0,3548	1,2230	2,704	0,105	-------	52060	---------
1	CuO + ZnO + NiO + Graphite + PCL	-0,2170	0,0143	0,970	0,202	98,83	4469000	98,84
2	ZnO + Graphite + PCL	-0,3089	0,1058	1,036	0,136	91,35	601900	91,35
3	ZnO + CuO + NiO + PCL	-0,2363	0,0335	0,955	0,213	97,26	1904000	97,27
4	PCL + ZnO	-0,3521	0,5663	2,085	0,094	53,70	112500	53,73
5	PCL + Graphite	-0,2797	0,1672	0,498	0,132	86,33	381000	86,34
6	2 fluorothiosemicarbazide + ZnO + PCL	-0,2953	0,6635	1,065	0,141	45,75	95990	45,77
7	4 fluorothiosemicarbazide + ZnO + NiO + CuO + PCL	-0,2903	0,5448	1,380	0,140	55,45	116900	55,46
8	2 fluorothiosemicarbazide + ZnO + NiO + CuO + PCL	-0,1913	0,0220	0,565	0,171	98,20	2896000	98,20
9	PCL	-0,2639	0,079	0,426	0,137	93,54	806100	93,54
10	4 fluorothiosemicarbazide + ZnO + PCL	-0,2700	0,725	0,245	0,079	40,72	86020	39,48

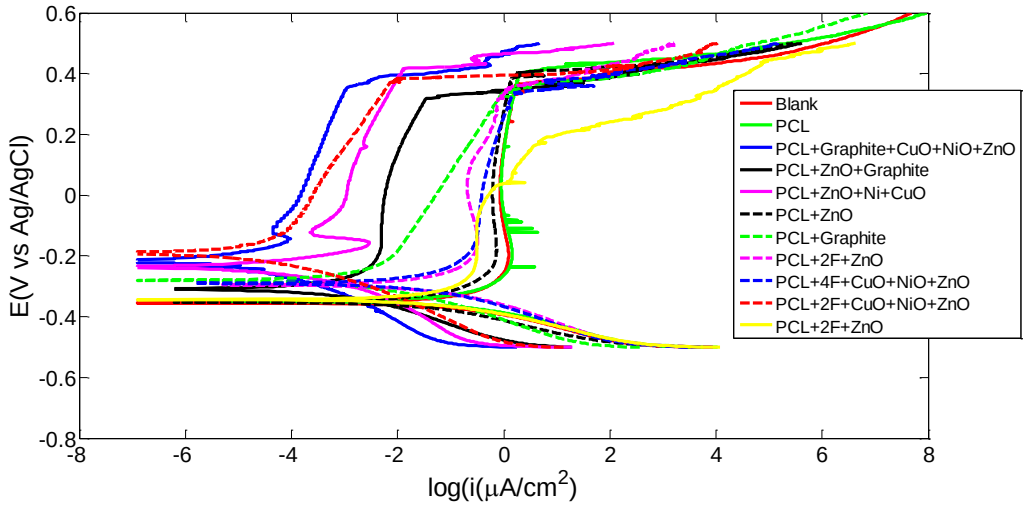

Figure 6 Tafel graphs of samples

An important evaluation method used to find E_{corr} and protection efficiency is the examination of the Tafel graph. According to evaluation of the intersection points at which the curves cross in the graph, sample 8 has the highest E_{corr} value (-0.1913), while the blank has the lowest E_{corr} value (-0.3548). In comparing the protection efficiency values, sample 1 shows best performance of the protection efficiency (%98.83) whereas sample 10 is the worst (% 40.72).

Table 2 Values of circuit components and total polarizations of samples (0: blank, 1-10: sample sequence number)

	Rs	R_{p1}	CPE_1 Q_1	n_1	R_{p2}	CPE_2 Q_2	n_2	R_{p3}	CPE_3 Q_3	n_3	R_{Tp}	W
0	9,07E+00	1,54E+04	1,58E+00	8,30E-01	1,88E+09	-	-	-	-	-	1,54E+04	
1	1,57E+01	1,91E+03	5,37E-10	9,99E-01	5,49E+06	8,54E-07	0.960 E+00	5,23E-03	2,52E+01	8,58E-01	5,49E+06	7,89E-07
2	1,03E+00	1,53E+07	3,96E-06	8,80E-01	8,85E+05	4,82E-06	8,46E-01	3,54E+02	3,45E-09	8,44E-01	1,62E+07	
3	1,26E+02	1,88E+07	1,13E-06	8,26E-01	4,15E+03	2,75E-06	7,15E+02	9,37E+01	1,04E-05	8,63E-01	1,88E+07	
4	2,91E+01	5,71E+05	1,13E-01	7,00E-01	7,47E+06	3,63E-05	9,22E-01	3,35E+06	1,23E-05	9,16E-01	1,14E+07	
5	3,47E+01	1,60E+06	1,29E-05	7,00E-01	6,22E+03	1,22E-05	7,00E-01	1,12E+02	1,51E-07	7,00E-01	1,61E+06	
6	3,30E+01	1,10E+02	8,07E-05	8,30E-01	2,87E+06	4,86E-05	8,42E-01	1,28E+04	1,16E-02	9,00E-01	2,88E+06	
7	3,20E+01	2,41E+08	6,84E-05	7,70E-01	3,27E+02	1,11E-02	0.99E+00	2,64E+06	2,72E-05	9,93E-01	2,43E+08	
8	1,65E+02	1,81E+08	1,98E-06	7,62E-01	1,03E+04	2,25E-06	7,00E-01	2,53E+02	2,60E-07	7,00E-01	1,81E+08	
9	2,77E+01	2,57E+02	6,17E-05	8,93E-01	6,21E+05	2,95E-05	9,12E-01	2,22E+06	6,26E-05	0.99E+00	2,84E+06	
10	3,16E+01	7,45E+06	4,87E-05	8,46E-01	4,54E+01	2,97E-01	7,00E-01	9,85E+01	9,71E-05	9,12E-01	7,45E+06	

Table 3 shows the equivalent circuits for blank and coated samples. As a constant phase element, CPE is defined by the phase shift n, which is indicative of the uniformity level of the substrate. To improve the accuracy of the experimental results, CPE was substituted for a double layer capacitance (C_{dl}) in the model. Rs represents the solution resistance, while

R1, R2, R3 and Rp1, Rp2 and Rp3 represent the polarization resistance. In addition to all circuit components, W1 exhibits Warburg impedance.

Table 3. Equivalent circuit models of the samples

Blank 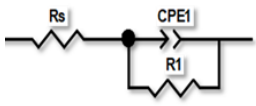	Sample 1 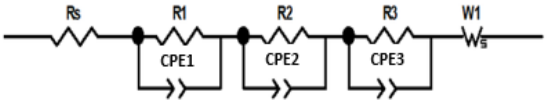
Sample 2, Sample 3, Sample 4, Sample 5, Sample 6, Sample 7, Sample 8, Sample 9, Sample 10 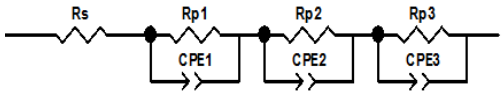	

CONCLUSIONS

In light of the data obtained from Nyquist plots, PCL + graphite + (ZnO, NiO, CuO) sample gives the best performance for corrosion inhibition of SS. In terms of performance, the PCL + Graphite + ZnO sample and the PCL + ZnO sample come after first one respectively.

Examining the Bode plots of the samples reveal that biggest breakpoint frequency value is reffered to PCL + (ZnO, NiO, CuO) sample. The others' breakpoint frequency values are close to each other.

Upon reviewing the Tafel data, PCL + graphite + (ZnO, CuO, NiO) sample has the best protection efficency percantage value among others. Second one is 2-floro thiosemicarbazide + PCL + (ZnO, CuO, NiO). Third one is PCL + (ZnO, CuO, NiO). The last one is 4-floro thiosemicarbazide + PCL + ZnO for protection efficiency percantage value.

In the case of equivalent circuit, Blank one have 1 resistance for solution, 1 CPE and 1 more resistance with parallel with CPE for modelling of circuit. For sample 1, circuit have 3 CPE, 3 resistance for parallel to CPE with individual match with one by one. Also there is a solution resistance and Warburg impedance for serial to CPE. From sample 2 to sample 10 have same circuit model which have 3 CPE, 3 polarization resistance and 1 solution resistance.

REFERENCES

1. Norman, P, Spack Daniel, E, Shumer N.J.N (2017) Physiological Implications of Myocardial Scar Structure. *Physiol. Behav.* https://doi.org/ 10.1177/0962280214537344.
2. Domínguez-Crespo, MA, Torres-Huerta, AM, González-Hernández, A, Brachetti-Sibaja, SB, Dorantes-Rosales, HJ, López-Oyama, AB (2018) Effect of deposition parameters on structural, mechanical and electrochemical properties in Ti/TiN thin films on AISI 316L substrates produced by r. f. magnetron sputtering. J. Alloys Compd.https://doi.org/10.1016/j.jallcom.2018.02.319.
3. Mojarad Shafiee, B, Torkaman, R, Mahmoudi, M, Emadi, R, Karamian, E (2019) An improvement in corrosion resistance of 316L AISI coated using PCL-gelatin composite by dip-coating method." Prog. Org. Coatings. https://doi.org/10.1016/j.porgcoat.2019.01.057.
4. Mohan, C, C, Prabhath A, Cherian A,M, Vadukumpully, S, Nair, V, S, Chennazhi, K, Menon, D (2015) Nanotextured stainless steel for improved corrosion resistance and biological response in coronary stenting. Nanoscale.https://doi.org/10.1039/c4nr05015k
5. Jones, J,E, Chen, M, Yu Q (2014) Corrosion resistance improvement for 316L stainless steel coronary artery stents by trimethylsilane plasma nanocoatings. J. Biomed. Mater. Res. - Part B Appl. Biomater. https://doi.org /10.1002/ jbm.b.33115.
6. Ţoţea, G, Ioniţă, D, Demetrescu, I (2014) ICP-MS determinations in sustaining corrosion data of 316 stainless steels in bioliquids. UPB Sci. Bull. Ser. B Chem. Mater. Sci.
7. Sista D (2021) New perspective of Nanofibers: Synthesis and Applications. Book Chapter. Nanofibers – Synthesis, Properties and Applications. Editor : Brjesh Kumar. IntechOpen. 10.5772/intechopen.92484
8. Shafiee B. J., Torkaman R., Mahmoudi M., Emadi R., Karamian E (2019) An improvement in corrosion resistance of 316L AISI coated using PCL-gelatin composite by dip-coating method. Prog. In Org. Coat. https://doi.org/10.1016/j.porgcoat.2019.01.057.
9. Behzadnasab, M, Mirabedini, S,M, Kabiri K, Jamali, S (2011) Corrosion performance of epoxy coatings containing silane treated ZrO_2 nanoparticles on mild steel in 3.5 % NaCl solution.

Corros. Sci. https://doi.org/10.1016/j.corsci.2010.09.026.

10. Wan T, F, Zhang J, C,M, Kim S,W, Park, Y, Yang, Kim K, H, Kwon S,H (2017) Enhanced Corrosion Resistance of PVD-CrN Coatings by ALD Sealing Layers Nanoscale Res. Lett. https://doi.org/10.1186/s11671-017-2020-1.
11. Bagherzadeh, M, Haddadi H, Iranpour M (2016) Electrochemical evaluation and surface study of magnetite/PANI nanocomposite for carbon steel protection in 3.5% NaCl. Prog. Org. Coatings. https://doi.org/10.1016/j.porgcoat.2016.08.011.
12. Bagherzadeh, M, Ghahfarokhi, Z,S, Yazdi, E,G (2016) Electrochemical and surface evaluation of the anti-corrosion properties of reduced graphene oxide. RSC Adv. 6, https://doi.org /10.1039/c5ra26948b.
13. Abd El-Lateef, H, M, Mohamed, I,M,A, Zhu, J, H, Khalaf, M,M (2020) An efficient synthesis of electrospun TiO2-nanofibers/Schiff base phenylalanine composite and its inhibition behavior for C-steel corrosion in acidic chloride environments. J. Taiwan Inst. Chem. Eng. https://doi.org/10.1016/j.jtice.2020.06.002.
14. Bakhsheshi-Rad, H,R, Akbari, M, Ismail, A, F, Aziz M, Hadisi, Z, Pagan, M, Daroonparvar, Chen, X (2019) Coating biodegradable magnesium alloys with electrospun poly-L-lactic acid-åkermanite-doxycycline nanofibers for enhanced biocompatibility, antibacterial activity, and corrosion resistance. Surf. Coatings Technol. https://doi.org/10.1016/j.surfcoat.2019.124898.
15. Panahi Z, Tamjid, E, Rezaei, M (2020) Surface modification of biodegradable AZ91 magnesium alloy by electrospun polymer nanocomposite: Evaluation of in vitro degradation and cytocompatibility. Surf. Coatings Technol., https://doi.org/10.1016/j.surfcoat.2020.125461.
16. Karimi, Kichi, M, Torkaman, R, Mohammadi, H, Toutounchi, A, Kharaziha, M, Alihosseini, F (2020) Electrochemical and in vitro bioactivity behavior of poly (ε-caprolactone) (PCL)-gelatin-forsterite nano coating on titanium for biomedical application. Mater. Today Commun. https://doi .org/10.1016/j.surfcoat.2020.125461.
17. Li, D, Xia, Y (2004) Electrospinning of nanofibers: Reinventing the wheel? Adv. Mater. https://doi.org/10.1002/adma.200400719.
18. Zhao, X, Yuan, S, Jin, Z, Zhu, Q, Zheng, Q, Jiang, Q, Song, H, Duan, J (2020) Fabrication of composite coatings with core-shell nanofibers and their mechanical properties, anticorrosive performance, and mechanism in seawater. Prog. Org.Coatings. https://doi.org/10.1016/j.porgcoat.2020.105893.
19. Alfalah, G, K, M, Kamberli, E, Abbar, A, H, Kandemirli, F, Saraçoğlu, M (2020) Corrosion performance of electrospinning nanofiber ZnO-NiO-CuO/ PCL coated on mild steel in acid solution. Surfaces and Interfaces. https://doi.org/10.1016/j.surfin.2020.100760.
20. Yang, X, Shao, C, Guan, H, Li, X, Gong, J (2004) Preparation and characterization of ZnO nanofibers by using electrospun PVA/zinc acetate composite fiber as precursor. Inorg. Chem. Commun., https://doi.org/10.1016/j.inoche.2003.10.035.
21. Guan, H, Shao C, Wen, S, Chen, J, Gong, X, Yang (2003) Preparation and characterization of NiO nanofibres via an electrospinning technique. Inorg. Chem. Commun. https://doi.org/10.1016/j.inoche.2003.08.003.